In the past, it has been difficult to trace such large-scale changes in body form to the action of particular genes and mutations. Our results show that large changes in vertebrate skeletal morphology in the wild can be created by relatively simple genetic mechanisms. Natural populations have variants of the same major signaling genes already known to play a crucial role in normal development and human disease. The variant alleles preexist at low frequency in ancestral marine populations and can be repeatedly fixed in new environments to produce a rapid shift to an alternative body form. Many other dramatic morphological, physiological, and behavioral changes are known in sticklebacks. With the recent advent of forward genetic approaches in this system, it should now be possible to identify the genes that underlie many ecologically important traits, which will bring a new molecular dimension to the study of how phenotypic changes arise during vertebrate evolution.

### References and Notes

1. D. J. Futuyma, *Evolutionary biology* (Sinauer Associates, Sunderland, MA, ed. 3, 1998).
2. D. Schluter, E. A. Clifford, M. Nemethy, J. S. McKinnon, *Am. Nat.* **163**, 809 (2004).
3. C. L. Peichel *et al.*, *Nature* **414**, 901 (2001).
4. P. F. Colosimo *et al.*, *PLoS Biol.* **2**, 635 (2004).
5. M. D. Shapiro *et al.*, *Nature* **428**, 717 (2004).
6. W. A. Cresko *et al.*, *Proc. Natl. Acad. Sci. U.S.A.* **101**, 6050 (2004).
7. D. M. Kingsley *et al.*, *Behavior* **141**, 1331 (2004).
8. M. A. Bell, S. A. Foster, Eds., *The Evolutionary Biology of the Threespine Stickleback* (Oxford Univ. Press, Oxford, 1994).
9. B. E. Deagle, T. E. Reimchen, D. B. Levin, *Can. J. Zool.* **74**, 1045 (1996).
10. G. L. Cuvier, M. A. Valenciennes, *Histoire naturelle des poissons: Tome quatrieme* (Chez F. G. Levrault, Paris, 1829).
11. D. W. Hagen, L. G. Gilbertson, *Evolution Int. J. Org. Evolution* **26**, 32 (1972).
12. N. Giles, *J. Zool.* **199**, 535 (1983).
13. E. B. Taylor, J. D. McPhail, *Can. J. Zool.* **64**, 416 (1986).
14. C. A. Bergstrom, *Can. J. Zool.* **80**, 207 (2002).
15. D. W. Hagen, L. G. Gilbertson, *Heredity* **30**, 273 (1973).
16. T. E. Reimchen, *Evol. Int. J. Org. Evol.* **46**, 1224 (1992).
17. T. E. Reimchen, *Behaviour* **137**, 1081 (2000).
18. D. G. Ransom, L. I. Zon, *Methods Cell Biol.* **60**, 195 (1999).
19. E. S. Lander, D. Botstein, *Cold Spring Harb. Symp. Quant. Biol.* **51**, 49 (1986).
20. J. C. Avise, *Genet. Res.* **27**, 33 (1976).
21. I. Thesleff, M. L. Mikkola, *Sci. STKE* **2002**, pe22 (2002).
22. A. T. Kangas, A. R. Evans, I. Thesleff, J. Jernvall, *Nature* **432**, 211 (2004).
23. S. Kondo *et al.*, *Curr. Biol.* **11**, 1202 (2001).
24. J. Y. Sire, A. Huysseune, *Biol. Rev. Camb. Philos. Soc.* **78**, 219 (2003).
25. K. Paakkonen *et al.*, *Hum. Mutat.* **17**, 349 (2001).
26. M. C. Vincent, V. Biancalana, D. Ginisty, J. L. Mandel, P. Calvas, *Eur. J. Hum. Genet.* **9**, 355 (2001).
27. M. Bayes *et al.*, *Hum. Mol. Genet.* **7**, 1661 (1998).
28. M. Yan *et al.*, *Science* **290**, 523 (2000).
29. J. Kere *et al.*, *Nature Genet.* **13**, 409 (1996).
30. M. L. Mikkola *et al.*, *Mech. Dev.* **88**, 133 (1999).
31. G. Orti, M. A. Bell, T. E. Reimchen, A. Meyer, *Evol. Int. J. Org. Evol.* **48**, 608 (1994).
32. E. B. Taylor, J. D. McPhail, *Biol. J. Linn. Soc.* **66**, 271 (1999).
33. M. Higuchi, A. Goto, *Environ. Biol. Fishes* **47**, 1 (1996).
34. A. K. Srivastava *et al.*, *Hum. Mol. Genet.* **10**, 2973 (2001).
35. K. E. Hosemann, P. F. Colosimo, B. R. Summers, D. M. Kingsley, *Behavior* **141**, 1345 (2004).
36. M. J. Heuts, *Evol. Int. J. Org. Evol.* **1**, 89 (1947).
37. J. MacLean, *Can. J. Zool.* **58**, 2026 (1980).
38. D. W. Hagen, *J. Fish. Res. Board Can.* **24**, 1637 (1967).
39. G. E. E. Moodie, J. D. McPhail, D. W. Hagen, *Behaviour* **47**, 95 (1973).
40. B. Schiemann *et al.*, *Science* **293**, 2111 (2001).
41. S. Williams-Blangero *et al.*, *Proc. Natl. Acad. Sci. U.S.A.* **99**, 5533 (2002).
42. C. J. Wei, X. Xu, C. W. Lo, *Annu. Rev. Cell Dev. Biol.* **20**, 811 (2004).
43. C. C. Lindsey, *Can. J. Zool.* **40**, 271 (1962).
44. We thank K. Peichel, J. McKinnon, B. Jónsson, F. von Hippel, M. Kalbe, S. Mori, K. Olivera, and members of the Kingsley laboratory for generous help with fish collecting and population samples; D. Schlessinger and V. Thermes for the pCI neo-Eda A1 and pIScel-pBSIISK+ plasmids; J. Weir for help with phylogenetic analysis; M. McLaughlin for fish care; and W. Talbot, K. Peichel, and lab members for useful comments on the manuscript. This work was supported in part by a Center of Excellence in Genomic Science grant from the National Institutes of Health (1P50HG02568; D.M.K., R.M.M.); the Ludwig Foundation (D.M.K.); and the Natural Sciences and Engineering Research Council and the Canada Foundation for Innovation (D.S.). D.S. is a Canada Research Chair, and D.M.K. is an Investigator of the Howard Hughes Medical Institute. This work is dedicated in fond memory of Kim Hosemann, a passionate and talented scientist who died a few months after completing the key transgenic experiments.

# Temporal Relationships of Carbon Cycling and Ocean Circulation at Glacial Boundaries

**Alexander M. Piotrowski,\*† Steven L. Goldstein, Sidney R. Hemming, Richard G. Fairbanks**

Evidence from high-sedimentation-rate South Atlantic deep-sea cores indicates that global and Southern Ocean carbon budget shifts preceded thermohaline circulation changes during the last ice age initiation and termination and that these were preceded by ice-sheet growth and retreat, respectively. No consistent lead-lag relationships are observed during abrupt millennial warming events during the last ice age, allowing for the possibility that ocean circulation triggered some millenial climate changes. At the major glacial-interglacial transitions, the global carbon budget and thermohaline ocean circulation responded sequentially to the climate changes that forced the growth and decline of continental ice sheets.

Records of past global climate preserve evidence of large-scale changes in temperature and ice volume at glacial-interglacial boundaries. Although the timing of ice ages is broadly driven by Milankovich orbital cycles, the small insolation changes require amplifying mechanisms to produce the large glacial-interglacial climate changes. Fluctuation in North Atlantic Deep Water (NADW) production is a potential amplifier and has been suggested as a trigger for rapid global climate shifts (1). Carbon dioxide ($CO_2$) is another possible amplifier on glacial-interglacial time scales, because its atmospheric concentration is predominantly controlled by changes in deep-ocean storage (2) and the terrestrial carbon reservoir (e.g., 3–5). Carbon isotope ratios are distinct in different reservoirs, making it a powerful tool to constrain the timing of global carbon budget reorganizations relative to other changes in the climate system. In the oceans, carbon isotope ratios of benthic foraminifera (benthic $\delta^{13}C$) are commonly used as a proxy for ocean circulation because they vary systematically in water masses [e.g., (6–8)]. However, temporal benthic $\delta^{13}C$ changes at any location reflect a combination of the global carbon mass balance, ocean-circulation changes, air-sea equilibration, and productivity changes. If carbon budget and ocean-circulation signals can be deconvolved, the temporal sequence of major shifts in global ice volume, carbon mass balance, and ocean circulation can help to clarify the ocean's role as a trigger of, or a response to, major climate changes. In this study, we compare the temporal sequence of these changes since the last interglacial period. Chronological ambiguities are obviated through study of different proxy signals in the same core, and thus the sequence of events associated with climate change and ocean circulation can be extracted.

**Nd isotopic systematics.** We use Nd isotopes as a proxy of the balance between NADW and southern-sourced waters in the South Atlantic. $^{143}Nd/^{144}Nd$ ratios vary in the

Lamont-Doherty Earth Observatory and Department of Earth and Environmental Sciences, Columbia University, Palisades, NY 10964, USA.

*Present address: Department of Earth Sciences, Cambridge University, Downing Street, Cambridge, CB2 3EQ, UK.
†To whom correspondence should be addressed. E-mail: apio04@esc.cam.ac.uk

Earth as a result of the α decay of $^{147}$Sm ($t_{1/2} \sim 106 \times 10^9$ years), and in the oceans, the values reflect the age of the continental sources of dissolved Nd (9). The utility of Nd isotopes as a paleocirculation proxy stems from its variability in the oceans. In seawater and Fe-Mn nodule and crust surfaces, Nd isotope ratios geographically vary over a large range from $\varepsilon_{Nd} < -20$ in the Labrador Sea to values as high as $\varepsilon_{Nd} \sim 0$ in the northwest Pacific (10). Unlike low-mass stable isotope and element ratios, Nd isotope ratios do not show measurable mass-dependent fractionation by biological and low-temperature processes (11). Nd isotopes are conservative in seawater unless new Nd is added along the transport path. Water-column profiles show that water masses conserve the Nd isotopic fingerprint of the dissolved Nd source regions over long transport paths. For example, the NADW Nd isotope signature ($\varepsilon_{Nd} \sim -14$) can be traced into the South Atlantic, and the Antarctic Bottom Water (AABW) signature ($\varepsilon_{Nd} \sim -7$ to $-9$) can be traced northward in the Atlantic (9, 12, 13).

The Nd isotopic signal of deep-water masses can be preserved at submillennial time resolution in the Fe-Mn oxide fraction of deep-sea cores, and recent studies found Nd isotopic variability in the oceans on glacial-interglacial and millennial time scales (14–18). This study

focuses on cores RC11-83 (40°36′S, 9°48′E, 4718 m) and TNO57-21 (41°08′S, 7°49′E, 4981 m) from the Cape Basin, southeast Atlantic (tables S1 and S2), whose chronology is based on radiocarbon ages and spliced stable isotope stratigraphy (8, 18–20). High sedimentation rates (~20 and ~15 cm/1000 years, respectively) allow subcentury-scale temporal resolution. An initial application of Nd isotope ratios of Fe-Mn leachates in RC11-83 at orbital time resolution (15) showed that the NADW signals were stronger during warmer climate intervals and weaker during cold intervals through the last ice age. These variations were subsequently confirmed in a Holocene to Last Glacial Maximum (LGM) profile of core MD96-2086 from the northern Cape Basin (16, 21). Our more detailed studies of RC11-83 and TNO57-21 show fine-scale variability that parallels other climate proxies (18) (Fig. 1). The previous studies include extensive discussions of evidence that Nd isotope ratios in the Fe-Mn oxide leachates of these cores reflect deep seawater (15, 16, 18, 22). In RC11-83/TNO57-21, Sr isotope ratios are indistinguishable from Quaternary seawater ($^{87}$Sr/$^{86}$Sr ~ 0.7092) and much lower than associated terrigenous detritus (0.717 to 0.723) (23). This precludes detrital contamination of the leached Sr. Nd is less likely to be contaminated by the detritus, because it is much less

soluble than Sr. Moreover, bottom-water $SiO_2$ concentrations (24) and core top leachate Nd isotope ratios are consistent with $\varepsilon_{Nd}$-$SiO_2$ co-variations of present-day Atlantic seawater (15).

**Climate transitions.** During Marine Isotope Stages (MIS) 1 and 5, Nd isotopes are the most NADW-like (Fig. 1), whereas during MIS 2 and 4 (full glacial stages), values shift beyond modern Southern Ocean values of $\varepsilon_{Nd} \sim -7$ to $-9$ (9), indicating that the Southern Ocean was more Pacific-like than today. Major Nd isotope shifts occurred at the MIS 5a/4 and 2/1 boundaries. Millennial excursions occur between MIS4/5 and the LGM, corresponding in timing and form to Greenland interstadials 3, 4, 8, 12, 14, and 17 on the basis of comparison to Greenland ice cores $\delta^{18}$O records (25–27). Piotrowski et al. (18) discuss the detailed temporal relationships between changes in Nd isotope ratios and Greenland ice $\delta^{18}$O during the most recent deglaciation. For example, there is increased NADW during the Bølling warming, a decline during the Allerød cooling, and an increase from the Younger Dryas minimum (labeled YD; see Fig. 1B) to the early Holocene. In contrast, there is no corresponding effect during the Antarctic Cold Reversal (ACR). These associations demonstrate a strong linkage between Northern Hemisphere climate variability and the Nd isotope ratios of South Atlantic deep waters.
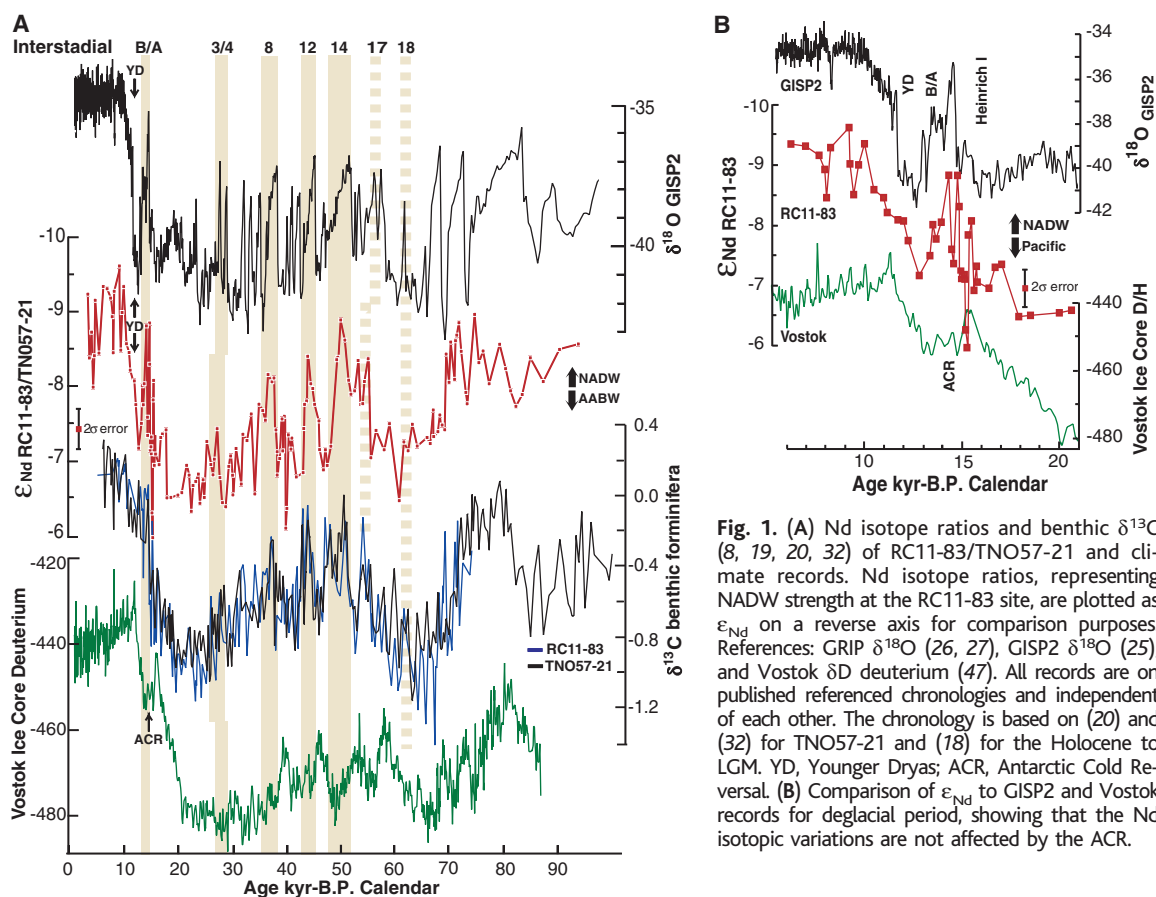


**Fig. 1. (A)** Nd isotope ratios and benthic $\delta^{13}$C (8, 19, 20, 32) of RC11-83/TNO57-21 and climate records. Nd isotope ratios, representing NADW strength at the RC11-83 site, are plotted as $\varepsilon_{Nd}$ on a reverse axis for comparison purposes. References: GRIP $\delta^{18}$O (26, 27), GISP2 $\delta^{18}$O (25), and Vostok $\delta$D deuterium (47). All records are on published referenced chronologies and independent of each other. The chronology is based on (20) and (32) for TNO57-21 and (18) for the Holocene to LGM. YD, Younger Dryas; ACR, Antarctic Cold Reversal. **(B)** Comparison of $\varepsilon_{Nd}$ to GISP2 and Vostok records for deglacial period, showing that the Nd isotopic variations are not affected by the ACR.

The covariation of the temporal patterns of benthic δ13C and Nd isotopes on long-term and millennial time scales (Fig. 1) confirms earlier conclusions that the benthic δ13C pattern mimics ocean-circulation changes (8, 19, 20). However, the magnitude of the benthic δ13C changes over glacial-interglacial cycles are too large to have been caused entirely by water-mass mixing. The mean δ13C of the deep ocean reflects the climate-forced partition of carbon between terrestrial and ocean carbon reservoirs. The deep ocean δ13C was 0.46‰ to 0.32‰ lower during ice ages than today (28–30), likely caused by increased storage of ~500 gigatons of terrestrial organic carbon (δ13C ~ –25‰) in the ocean (31). The interglacial to glacial benthic δ13C shift of ~–0.8‰ in RC11-83/TNO57-21 overshoots the glacial Pacific end member by ~–0.4‰ (32–34), which reflects additional productivity and perhaps air-sea exchange and local pore-water effects in the Southern Ocean (35).

To isolate the noncirculation effects on the benthic δ13C signal, we use Nd isotopes to monitor thermohaline circulation and interpret the δ13C shifts that are unsupported by the Nd isotope record as caused by noncirculatory effects. A cross-plot of the entire data set is compared to Holocene and glacial binary mixing curves for global end-member water masses (Fig. 2A). The Nd isotope ratios fall between the NADW and Pacific end members throughout, whereas the δ13C data lie below the mixing lines and shift beyond the glacial Pacific value during glacial climate. The NADW-Pacific mixing lines are an over-simplification of the ocean-circulation system (Fig. 2), which we regard as reference lines

allowing a first-order evaluation of large non-circulation effects on Southern Ocean δ13C. They assume that the temporal variability of the Nd isotope ratios is not controlled by shifts in the end-member water masses. Our previous studies extensively discuss the current constraints on the Pacific and North Atlantic end members (15, 18) and are only summarized here. There is strong evidence for stability of Nd isotope ratios of deep Pacific seawater (36). Constraining the Nd isotope ratio of NADW through time is more problematic because of encroachment of AABW into the North Atlantic during cold climate and shallowing of northern-sourced deep waters and the failure of Fe-Mn oxides leached from many North Atlantic cores to yield marine Sr isotope ratios (37). Rutberg et al. [figure 2a in (15)] addressed the issue indirectly by comparing bottom-water $SiO_2$ concentrations (24) and Nd isotope ratios in global Fe-Mn nodules and crusts with the modern seawater-dissolved $SiO_2$-$\varepsilon_{Nd}$ trend. Samples from Fe-Mn nodules and crusts represent average ambient water values over $10^5$ to $10^6$ years, encompassing several glacial cycles. Most of the North Atlantic data lie on the modern $SiO_2$-$\varepsilon_{Nd}$ trend, indicating a roughly constant NADW Nd isotope signature. Recent suggestions that the Nd isotope signature of glacial NADW may have been lower (e.g., 38–40) than the present day would not affect our primary conclusions (41).

Further insights into the Nd isotope–benthic δ13C relationships are gained by separating the data into discrete time slices. Although all the data (Fig. 2A) show a negative correlation, the glacial-interglacial transitions (MIS 5a/4 and LGM-Holocene)

data outline a "parallelogram" (Fig. 2B), and those from the MIS 4/3 through the LGM fill its gap (Fig. 2C). Further examination shows that the parallelogram reflects the temporal relationships between Nd and carbon isotope shifts. For example, the data associated with the last deglaciation (Fig. 3A) exhibit a two-stage change. The LGM to Bølling warming data lie on a steep trend, because the δ13C undergoes a major change toward its Holocene range, whereas the Nd isotopes show a small shift. The benthic δ13C increases by 0.8‰, representing 90% of the total LGM to Holocene shift, whereas the Nd isotopes decrease by ~–0.6 $\varepsilon_{Nd}$ units, representing only ~15% of its total shift. The shallow trend of the post-Bølling data reflects the major glacial-interglacial Nd isotope shift occurring after the benthic δ13C had already shifted to the interglacial mode. These observations indicate that the $\varepsilon_{Nd}$-δ13C coupling before the Bølling warming was distinct from that afterward. The pre-Bølling interval was associated with substantial climate amelioration and glacial retreat in Europe (42). The data indicate that for ~1500 years before the Bølling warming (43), initial melting of the continental ice sheets was associated with large changes in the deep-water δ13C and small variations in deep-water circulation.

Deep-water δ13C shifted before the Bølling warming, at which time it had already attained its Holocene composition. After the Bølling warming, benthic δ13C was primarily affected by changes in the balance of the water masses. The shallow slope of the mixing curves (Fig. 2) illustrates that Nd isotopes are a more sensitive proxy for water-mass mixing than benthic
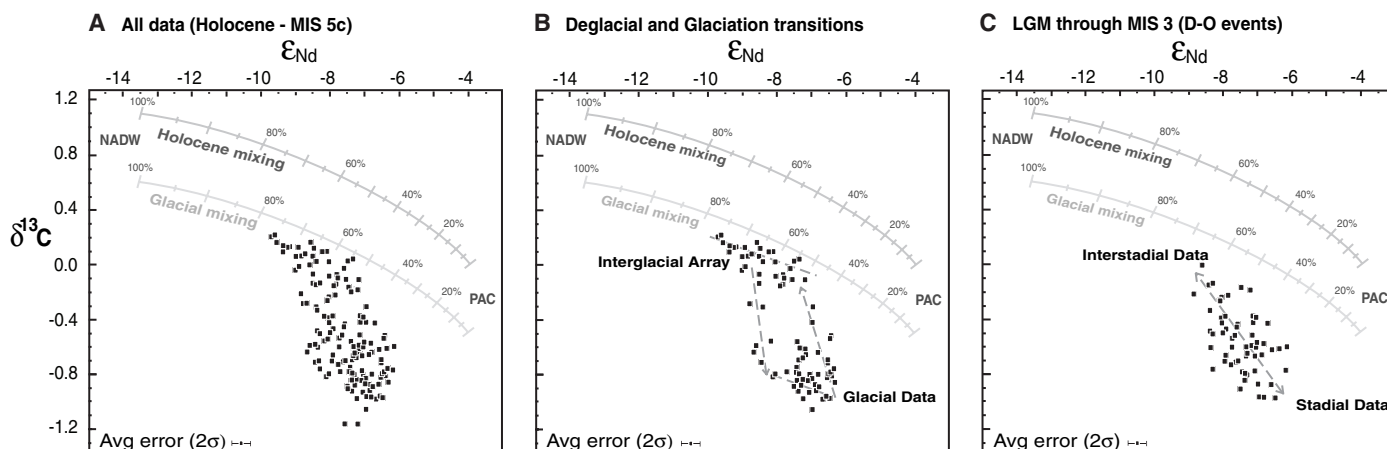


**Fig. 2.** Cross-plot of Nd isotope data and benthic δ13C of RC11-83/TNO57-21. (**A**) The entire 100,000-year record. (**B**) Only the glaciation (MIS 5a-4) and deglacial (LGM-Holocene) transitions. (**C**) Only glacial interstadial events (within MIS 3 and early MIS 2). Simple binary mixing curves are shown between NADW and Pacific (PAC) isotopic end members for the Holocene and the LGM; the δ13C difference between them is the 0.4‰ mean ocean δ13C difference (28–30) due to ocean-biosphere carbon budget change (31). The Nd isotopes and benthic δ13C recorded by RC11-83/TNO57-21 are monitoring the relative mixing proportion of NADW and Pacific-sourced waters in the Southern Ocean (changes in which should parallel the mixing reference curves), whereas benthic δ13C is also affected by noncirculatory carbon budget changes. Dashed arrows show sequential Nd isotope-benthic δ13C changes relative to general ocean mixing (Fig. 3). NADW-Pacific mixing curves are based on the following parameters. For the Holocene end members, –NADW: $\varepsilon_{Nd}$ = –13.5, Nd = 21 pmol/kg, δ13C = 1.1, dissolved $CO_2$ = 2175 umol/kg; Pacific: $\varepsilon_{Nd}$ = –4, Nd = 40 pmol/kg, δ13C = 0.0, dissolved $CO_2$ = 2350 umol/kg. For the Glacial end members, NADW: δ13C = 0.6; Pacific: δ13C = –0.5; all other parameters are the same. Mixing curves are based on (32–34, 48–51). Benthic δ13C are from (8, 19, 20, 32).
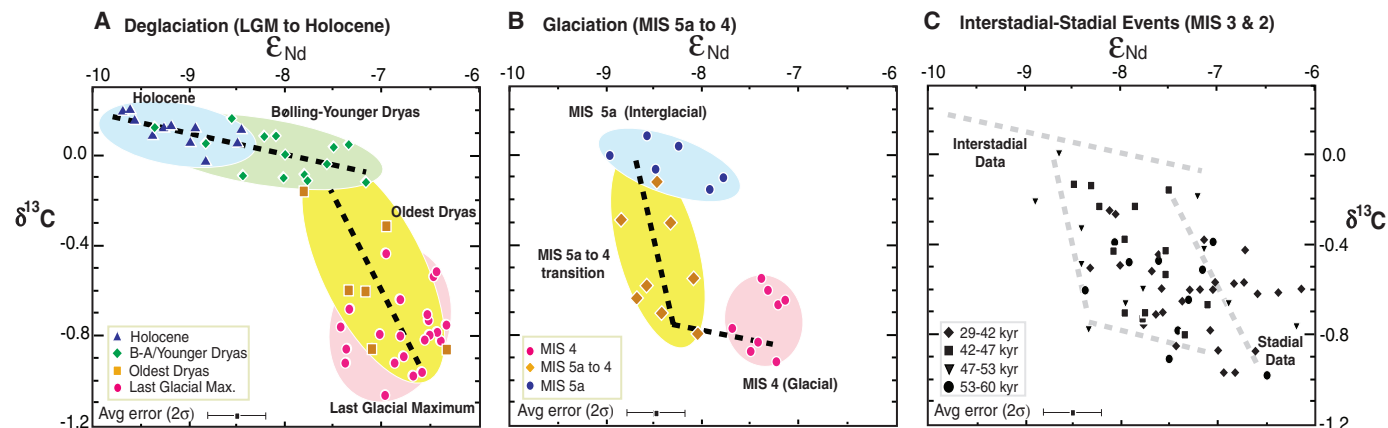
**Fig. 3.** Nd isotope ratios versus benthic $\delta^{13}C$ further separated into distinct time slices. (**A**) Deglaciation interval (LGM-Holocene). (**B**) The last glaciation (MIS 5a-4). (**C**) Major MIS 3 and early MIS 2 interstadial-stadial events. Scales differ from Fig. 2. Dashed lines in (A) and (B) indicate sequential changes during glacial-interglacial transitions and are reproduced in (C) to illustrate that during major interstadial-stadial events, bottom-water carbon and Nd isotopes shifted from glacial compositions toward interglacial compositions and back again, without the same lead-lag relationship as glacial-interglacial transitions.

$\delta^{13}C$. The Bølling warming to Holocene trend nearly parallels the NADW-Pacific mixing lines, whereas LGM to Bølling warming data comprise a steeper slope (Fig. 3A). This is why Nd isotopes record a large Younger Dryas change, whereas Charles *et al.* (*8*) found only a hint of a benthic $\delta^{13}C$ change. During the Younger Dryas, the range of $\varepsilon_{Nd}$ values approaches that of the entire shift from the LGM to the Holocene without a comparable benthic $\delta^{13}C$ shift (Fig. 3A). A 20% reduction of NADW after the Bølling warming produces an increase in the Nd isotope ratio of ~2 $\varepsilon_{Nd}$ units, with only a ~0.2‰ change in $\delta^{13}C$.

The sequence of events during the last interglacial-glacial transition (MIS 5a to 4) is identical to the deglacial sequence, with benthic $\delta^{13}C$ shifting toward glacial values before Nd isotopes (Fig. 3B), manifested by a steep trend followed by a shallow one, a mirror image of the deglacial transition. In the initial steep trend, the decrease in benthic $\delta^{13}C$ values is equal in magnitude to the deglaciation shift, without a significant change in Nd isotope ratios. Subsequently, a rapid $\varepsilon_{Nd}$ shift occurred, resulting in the shallow trend, consistent with a reduction in NADW intensity. The MIS 5a/4 NADW shift lags the benthic $\delta^{13}C$ shift by ~2,500 years (corresponding to 27 cm in TNO57-21). As discussed above for the Younger Dryas, water-mass mixing dynamics is also responsible for the small $\delta^{13}C$ change compared with the natural scatter that accompanies the abrupt Nd isotope shift during the MIS 5a-4 transition (Fig. 4).

The comparisons of Nd and benthic carbon isotopes have important implications for the sequence of events at major climate transitions. The data indicate that during the last glaciation and deglaciation, major changes in South Atlantic deep-water $\delta^{13}C$ occurred prior to major changes in the global overturning circulation.

Significant variability in Nd and benthic $\delta^{13}C$ also occurred during the millennial

Dansgaard-Oeschger (D-O) interstadial warmings of MIS 3 and early MIS 2 (Fig. 1), which fill the parallelogram formed by the glacial-interglacial transition data (Fig. 2 and Fig. 3C). During interstadials, the data shifts directly from full glacial values (higher $\varepsilon_{Nd}$ and lower $\delta^{13}C$) toward the NADW end member, although there is some scatter. Here, the carbon and ocean-circulation changes do not display a consistent two-stage lead-lag relationship as during the main glacial-interglacial transitions (Fig. 3C). This simple relationship shows that benthic $\delta^{13}C$ and Nd isotopes were responding synchronously to circulation changes during MIS 3 and early MIS 2, which (unlike the glacial-interglacial transitions) may allow for a causal role for ocean circulation to trigger the interstadial warmings.

It is unlikely that the consistent benthic $\delta^{13}C$ lead over $\varepsilon_{Nd}$ at the glacial-interglacial boundaries was produced by bioturbation or diagenesis. The benthic $\delta^{13}C$ record was generated on *Cibicidoides wüllerstorfi*, which live at or above the sediment-water interface. Processes that might affect the relative position of benthic $\delta^{13}C$ and $\varepsilon_{Nd}$ changes include seawater intrusion into sediment porewaters, bioturbation, and postdepositional smearing of the Fe-Mn oxides. Precipitation of Fe-Mn oxides from bottom-water–derived porewaters at depth within the sediment column would cause the Nd isotope record to lead, rather than lag, the benthic $\delta^{13}C$ record, opposite to what we observe. Bioturbation could cause downward mixing of foraminifera relative to other substrates containing Fe-Mn oxide coatings. If this occurred, the depth difference would have to be >20 cm (the lead-lag depth difference of glacial-interglacial Nd and benthic $\delta^{13}C$ changes), which is highly unlikely. The overall RC11-83/TNO57-21 $\varepsilon_{Nd}$ and benthic $\delta^{13}C$ profiles (Fig. 1) give strong evidence against smearing of Fe-Mn oxides generating the lag in Nd isotope changes during

the transitions. First, the glacial-interglacial changes are abrupt. Second, there is no lead-lag relationship during millennial fluctuations throughout the record. During most millennial events, benthic $\delta^{13}C$-$\varepsilon_{Nd}$ covary on centimeter scales [e.g., the "false start" at 15.5 thousand years before the present (ky cal. B.P.), 277 cm (*8*)]. We conclude that the carbon and Nd isotope data and their lead-lag relationship at major stage boundaries reflect bottom-water chemistry changes at this site.

**Temporal relationships.** The temporal relationship between the benthic $\delta^{13}C$ and Nd isotopes indicates that the $\delta^{13}C$ of the deep South Atlantic shifted by 0.8‰ during glacial-interglacial transitions at ~1000 to 3000 years before changes in the balance between northern- and southern-sourced waters. The abruptness of the early benthic $\delta^{13}C$ shifts strongly indicates that they include both the glacial-interglacial mean ocean carbon isotope change of ~0.4‰ (*28–30*) and an additional ~0.4‰ reflecting processes related to Southern Ocean productivity or air-sea equilibration of carbon isotopes. If the mean ocean and Southern Ocean $\delta^{13}C$ shifts occurred separately, the record would show two steps rather than the single abrupt shift seen clearly during the last interglacial-glacial transition (Fig. 4). Moreover, all other ~0.4‰ $\delta^{13}C$ shifts are supported by Nd isotopes changes and, therefore, are attributable to circulation change. Although we are currently unable to quantitatively separate the different noncirculatory effects on the $\delta^{13}C$ record, the data strongly indicate that the Southern Ocean and mean ocean $\delta^{13}C$ changed simultaneously and before ocean circulation.

As the mean ocean $\delta^{13}C$ change was caused by redistribution of terrestrial biosphere and deep-ocean carbon, the relationship between $\delta^{13}C$ and Nd isotopes during the MIS 2/1 and 5/4 transitions implies that the transfer of isotopically light terrestrial
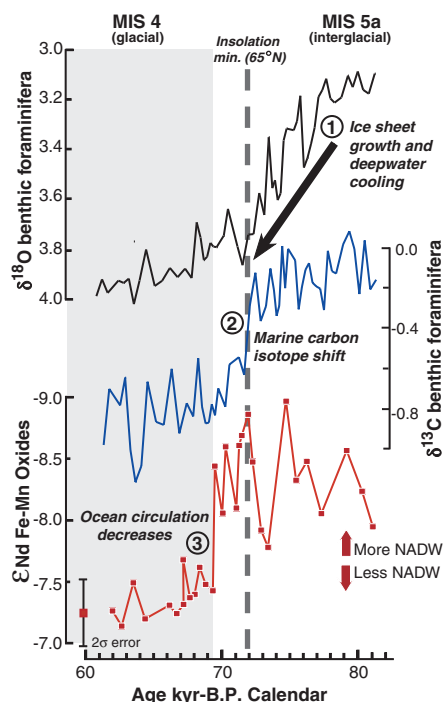
**Fig. 4.** Detail of MIS 5a/4 transition of benthic $\delta^{18}O$, benthic $\delta^{13}C$ (20, 32), and Nd isotope records in core TNO57-21. Sequential events include the benthic $\delta^{18}O$ change signifying nucleation and growth of continental ice sheets and cooler bottom waters; the major shift in benthic $\delta^{13}C$, unsupported by Nd isotopes and attributed to a noncirculatory signal from carbon budget reorganization; and the $\epsilon_{Nd}$ shift reflecting reduction of the NADW signal to glacial levels. The dashed line at 72 ky B.P. corresponds to the $\delta^{13}C$ shift as well as a minimum in Northern Hemisphere insolation. Ages were assigned by matching the benthic $\delta^{18}O$ to SPECMAP (52) by (20, 32). However, since all three records are from the same core, the sequences of events are directly comparable.

carbon between these reservoirs occurred prior to the shift between glacial-interglacial modes of ocean circulation. Because the terrestrial biosphere primarily responds to climate change, this strongly indicates that glacial-interglacial climate change occurred before changes in thermohaline circulation. The sequence of events during the MIS 5/4 transition can be shown by using benthic $\delta^{18}O$, benthic $\delta^{13}C$, and Nd isotopes to constrain the timing of ice-sheet growth and deep-water temperature, budget changes, and thermohaline circulation, respectively (Fig. 4). The growth of continental ice sheets is the primary cause of the benthic $\delta^{18}O$ change (32), which occurs first and is followed by a large benthic $\delta^{13}C$ shift (32) a few thousand years later, which is then followed by the Nd isotope shift. Colder deep-water temperatures causing a large portion of the glacial-interglacial $\delta^{18}O$ shift is also consistent with the establishment of glacial conditions concurrent with still-strong Atlantic overturning,

followed by a reduction of thermohaline circulation (44). The sequence of events for the last deglaciation is not as easily seen because of complex millennial-scale variations, although the early deglacial carbon shift compared with the Nd isotope shift shows up well in the benthic $\delta^{13}C$–$\epsilon_{Nd}$ cross-plots (45). The glaciation sequence shows that only after the growth of large continental ice sheets and a reorganization of both the global and Southern Ocean carbon budget was a weaker ocean-circulation regime established.

**Conclusions.** Comparison of proxies from a single core thus yields a temporal sequence of major climate events for the last glacial initiation and termination. During the last glaciation, climate and ice volume changed first, followed by the global carbon budget, which was in turn followed by ocean circulation. During deglaciation, the global carbon budget changed before ocean circulation strengthened. These temporal sequences show that thermohaline circulation changes did not trigger ice-sheet changes and global carbon budget reorganization. During the glaciation, strong ocean circulation and maritime conditions in the North Atlantic likely provided an important source of moisture for continental ice-sheet growth during the sustained cold conditions associated with the Northern Hemisphere insolation minimum at ~72 ky B.P. During interstadials through the last ice age, on the other hand, simultaneous changes in benthic $\delta^{13}C$ and Nd isotope ratios allow for the possibility of an ocean-circulation trigger for these millennial interstadial warmings. The observation that ice-sheet growth and global carbon cycle shifts precede ocean circulation changes at major glacial-interglacial boundaries shows that thermohaline circulation was a later amplifier but not the primary instigator of glacial-interglacial climate change.

**References and Notes**
1. W. S. Broecker, *Prog. Oceanogr.* **2**, 151 (1982).
2. W. S. Broecker, *The Glacial World According to Wally* (Eldigio Press, Palisades, NY, ed. 3, 2002).
3. J. M. Adams, H. Faure, L. Fauredenard, J. M. McGlade, F. I. Woodward, *Nature* **348**, 711 (1990).
4. J. M. Adams, W. M. Post, *Global Planet. Change* **20**, 243 (1999).
5. T. J. Crowley, *Global Biogeochem. Cycle* **9**, 377 (1995).
6. W. B. Curry, G. P. Lohmann, *Quat. Res.* **18**, 218 (1982).
7. D. W. Oppo, R. G. Fairbanks, *Earth Planet. Sci. Lett.* **86**, 1 (1987).
8. C. D. Charles, R. G. Fairbanks, *Nature* **355**, 416 (1992).
9. S. L. Goldstein, S. R. Hemming, in *Treatise on Geochemistry*, H. Elderfield, Ed. (Elsevier, Oxford, 2003), vol. 6, pp. 453–489.
10. F. Albarède, S. L. Goldstein, *Geology* **20**, 761 (1992).
11. The $\epsilon_{Nd}$ is the deviation of the $^{143}Nd/^{144}Nd$ of a sample from the bulk Earth value of 0.512638 (46) in parts per 10,000. The high-atomic-masses Nd isotopes (142 to 150 atomic mass units) and their single oxidation state (+3) inhibit significant mass-dependent fractionation. Moreover, corrections applied during mass-spectrometry measurement eliminate effects of any natural mass-dependent fractionation.
12. F. von Blanckenburg, *Science* **286**, 1862 (1999).
13. M. Frank, *Rev. Geophys.* **40**, 1001 (2002); 10.1029/2000RG000094.
14. K. W. Burton, D. Vance, *Earth Planet. Sci. Lett.* **176**, 425 (2000).
15. R. L. Rutberg, S. R. Hemming, S. L. Goldstein, *Nature* **405**, 935 (2000).
16. G. Bayon et al., *Chem. Geol.* **187**, 179 (2002).
17. D. Vance et al., *Paleoceanography* **19**, PA2009 (2004).
18. A. M. Piotrowski, S. L. Goldstein, S. R. Hemming, R. G. Fairbanks, *Earth Planet. Sci. Lett.* **225**, 205 (2004).
19. C. D. Charles, J. Lynch-Stieglitz, U. S. Ninnemann, R. G. Fairbanks, *Earth Planet. Sci. Lett.* **142**, 19 (1996).
20. U. S. Ninnemann, C. D. Charles, D. A. Hodell, in *Mechanisms of Global Climate Change at Millennial Time Scales* (American Geophysical Union, Washington, DC, 1999), vol. Geophysical Monograph 112, pp. 99–112.
21. The Sr isotopes and rare-earth-element patterns of leaches from this core match that of seawater, which is evidence for a marine rather than detrital origin for the Nd isotopes.
22. G. Bayon, C. German, R. Burton, R. Nesbitt, N. Rogers, *Earth Planet. Sci. Lett.* **224**, 447 (2004).
23. R. L. Rutberg, S. L. Goldstein, S. R. Hemming, R. Anderson, L. Burckle, *Paleoceanography*, in press.
24. S. Levitus, R. Burgett, T. Boyer, in *NOAA Atlas NESDros. Inf. Serv.* (U.S. Department of Commerce, Washington, DC, 1994), vol. 3.
25. P. M. Grootes, M. Stuiver, *J. Geophys. Res.* **102**, 26455 (1997).
26. G. R. I. P. Members, *Nature* **364**, 203 (1993).
27. S. J. Johnsen et al., *J. Geophys. Res.* **102**, 26397 (1997).
28. W. B. Curry, J. C. Duplessy, L. D. Labeyrie, N. J. Shackleton, *Paleoceanography* **3**, 317 (1988).
29. E. A. Boyle, *Annu. Rev. Earth Planet. Sci.* **20**, 245 (1992).
30. J. C. Duplessy et al., *Paleoceanography* **3**, 343 (1988).
31. U. Siegenthaler, in *Global Changes of the Past*, R. S. Bradley, Ed. (Univ. Corporation for Atmospheric Research, Boulder, CO, 1991), pp. 245–260.
32. U. S. Ninnemann, C. D. Charles, *Earth Planet. Sci. Lett.* **201**, 383 (2002).
33. K. Matsumoto, T. Oba, J. Lynch-Stieglitz, H. Yamamoto, *Quat. Sci. Rev.* **21**, 1693 (2002).
34. K. Matsumoto, J. Lynch-Stieglitz, *Paleoceanography* **14**, 149 (1999).
35. A. Mackensen, H. W. Hubberten, T. Bickert, G. Fischer, D. K. Futterer, *Paleoceanography* **8**, 587 (1993).
36. W. Abouchami, S. L. Goldstein, S. J. G. Galer, A. Eisenhauer, A. Mangini, *Geochim. Cosmochim. Acta* **61**, 3957 (1997).
37. A. M. Piotrowski, thesis, Columbia Univ. (2004).
38. C. Innocent, N. Fagel, R. K. Stevenson, C. Hillaire-Marcel, *Earth Planet. Sci. Lett.* **146**, 607 (1997).
39. N. Fagel, C. Innocent, R. K. Stevenson, C. Hillaire-Marcel, *Paleoceanography* **14**, 777 (1999).
40. F. von Blanckenburg, T. F. Nagler, *Paleoceanography* **16**, 424 (2001).
41. If the Nd isotope ratio of the North Atlantic end member decreased and the Pacific end member remained constant at the time of the major $\delta^{13}C$ change during the glaciation, it would be possible to buffer the Nd isotope ratio of South Atlantic deep water despite a weakening of thermohaline circulation. For example, the $\epsilon_{Nd}$ of NADW would have to shift from $\epsilon_{Nd} = -14$ to $-18$ in concert with the MIS 5a/4 $\delta^{13}C$ change (Fig. 1) and then rapidly shift back to $-14$ when we observe the change in the Nd isotope ratios. A complementary abrupt shift to $-10$ and then another shift back to $-14$ could explain the apparent $\delta^{13}C$ lead during the deglaciation. Although such scenarios, and variations thereof, cannot be completely ruled out, they require coincidental end-member $\epsilon_{Nd}$ and $\delta^{13}C$ shifts in both magnitude and timing, such that the $\epsilon_{Nd}$ at the core sites remain roughly constant. Thus, they would require evidence before they can be considered seriously. On the longer term, as explained in the text, there is good evidence that the Pacific end member remained nearly constant on glacial-interglacial time scales, whereas the North Atlantic end member is less well constrained, but current evidence indicates near constancy (15, 18).

42. G. H. Denton *et al.*, *Geogr. Ann. Ser. A Phys. Geogr.* **81A**, 107 (1999).

43. A 35-cm interval in RC11-83, which has an average sedimentation rate through this section of 24 cm/1000 years [a 29-cm interval in RC11-83 (*19, 20*)], would correspond to a time period of 1450 years.

44. W. F. Ruddiman, *Quat. Sci. Rev.* **22**, 1597 (2003).

45. Most Nd and carbon isotope measurements in the deglacial and Bølling warming portion of the record were not made on the same sample depths or splits. We therefore conservatively confine our interpretations to lead-lag relationships >150 years or >3 cm of core length.

46. S. B. Jacobsen, G. J. Wasserburg, *Earth Planet. Sci. Lett.* **50**, 139 (1980).

47. J. Jouzel *et al.*, *Nature* **329**, 403 (1987).

48. D. J. Piepgras, S. B. Jacobsen, *Geochim. Cosmochim. Acta* **52**, 1373 (1988).

49. D. J. Piepgras, G. J. Wasserburg, *Geochim. Cosmochim. Acta* **51**, 1257 (1987).

50. C. Jeandel, *Earth Planet. Sci. Lett.* **117**, 581 (1993).

51. D. Hodell, K. A. Venz, C. D. Charles, U. S. Ninnemann, *Geochem. Geophys. Geosyst.* **4**, 1 (2003).

52. D. G. Martinson *et al.*, *Quat. Res.* **27**, 1 (1987).

53. This manuscript benefited from discussions with R. Anderson, S. Barker, W. Broecker, H. Elderfield, E. Martin, J. McManus, U. Ninnemann, H. Scher, and A. Tripati; laboratory assistance from D. Zylberberg; and comments by anonymous reviewers. This study was supported by NSF grants OCE 98-09253 and OCE

# REPORTS

# A New Population of Very High Energy Gamma-Ray Sources in the Milky Way

F. Aharonian,[1] A. G. Akhperjanian,[2] K.-M. Aye,[3] A. R. Bazer-Bachi,[4] M. Beilicke,[5] W. Benbow,[1] D. Berge,[1] P. Berghaus,[6*] K. Bernlöhr,[1,7] C. Boisson,[8] O. Bolz,[1] C. Borgmeier,[7] I. Braun,[1] F. Breitling,[7] A. M. Brown,[3] J. Bussons Gordo,[9] P. M. Chadwick,[3] L.-M. Chounet,[10] R. Cornils,[5] L. Costamante,[1] B. Degrange,[10] A. Djannati-Ataï,[6] L. O'C. Drury,[11] G. Dubus,[10] T. Ergin,[7] P. Espigat,[6] F. Feinstein,[9] P. Fleury,[10] G. Fontaine,[10] S. Funk,[1†] Y. A. Gallant,[9] B. Giebels,[10] S. Gillessen,[1] P. Goret,[12] C. Hadjichristidis,[3] M. Hauser,[13] G. Heinzelmann,[5] G. Henri,[14] G. Hermann,[1] J. A. Hinton,[1] W. Hofmann,[1] M. Holleran,[15] D. Horns,[1] O. C. de Jager,[15] I. Jung,[1,13‡] B. Khélifi,[1] Nu. Komin,[7] A. Konopelko,[1,7] I. J. Latham,[3] R. Le Gallou,[3] A. Lemière,[6] M. Lemoine,[10] N. Leroy,[10] T. Lohse,[7] A. Marcowith,[4] C. Masterson,[1] T. J. L. McComb,[3] M. de Naurois,[16] S. J. Nolan,[3] A. Noutsos,[3] K. J. Orford,[3] J. L. Osborne,[3] M. Ouchrif,[16] M. Panter,[1] G. Pelletier,[14] S. Pita,[6] G. Pühlhofer,[1,13] M. Punch,[6] B. C. Raubenheimer,[15] M. Raue,[5] J. Raux,[16] S. M. Rayner,[3] I. Redondo,[10§] A. Reimer,[17] O. Reimer,[17] J. Ripken,[5] L. Rob,[18] L. Rolland,[16] G. Rowell,[1] V. Sahakian,[2] L. Saugé,[14] S. Schlenker,[7] R. Schlickeiser,[17] C. Schuster,[17] U. Schwanke,[7] M. Siewert,[17] H. Sol,[8] R. Steenkamp,[19] C. Stegmann,[7] J.-P. Tavernet,[16] R. Terrier,[6] C. G. Théoret,[6] M. Tluczykont,[10] D. J. van der Walt,[15] G. Vasileiadis,[9] C. Venter,[15] P. Vincent,[16] B. Visser,[15] H. J. Völk,[1] S. J. Wagner[13]

Very high energy γ-rays probe the long-standing mystery of the origin of cosmic rays. Produced in the interactions of accelerated particles in astrophysical objects, they can be used to image cosmic particle accelerators. A first sensitive survey of the inner part of the Milky Way with the High Energy Stereoscopic System (HESS) reveals a population of eight previously unknown firmly detected sources of very high energy γ-rays. At least two have no known radio or x-ray counterpart and may be representative of a new class of "dark" nucleonic cosmic ray sources.

Very high energy (VHE) γ-rays with energies $E > 10^{11}$ eV are probes of the nonthermal universe, providing access to energies far greater than those that can be produced in accelerators on Earth. The acceleration of electrons or nuclei in astrophysical sources leads inevitably to the production of γ-rays by the decay of $\pi^0$s produced in hadronic inter-

actions, inverse Compton scattering of high-energy electrons on background radiation fields, or the nonthermal bremsstrahlung of energetic electrons. Several classes of objects in the Galaxy are suspected or known particle accelerators: pulsars and their pulsar wind

[1]Max-Planck-Institut für Kernphysik, Post Office Box 103980, D-69029 Heidelberg, Germany. [2]Yerevan Physics Institute, 2 Alikhanian Brothers Street, 375036 Yerevan, Armenia. [3]Department of Physics, University of Durham, South Road, Durham DH1 3LE, UK. [4]Centre d'Etude Spatiale des Rayonnements, CNRS/UPS, 9 av. du Colonel Roche, BP 4346, F-31029 Toulouse Cedex 4, France. [5]Institut für Experimentalphysik, Universität Hamburg, Luruper Chaussee 149, D-22761 Hamburg, Germany. [6]Physique Corpusculaire et Cosmologie, IN2P3/CNRS, Collège de France, 11 Place Marcelin Berthelot, F-75231 Paris Cedex 05, France. [7]Institut für Physik, Humboldt-Universität zu Berlin, Newtonstr. 15, D-12489 Berlin, Germany. [8]Laboratoire Univers et Théories (LUTH), UMR 8102 du CNRS, Observatoire de Paris, Section de Meudon, F-92195 Meudon Cedex, France. [9]Groupe d'Astroparticules de Montpellier, IN2P3/CNRS, Université Montpellier II, CC85, Place Eugène Bataillon, F-34095 Montpellier Cedex 5, France. [10]Laboratoire Leprince-Ringuet, IN2P3/CNRS, Ecole Polytechnique, F-91128 Palaiseau, France. [11]Dublin Institute for Advanced Studies, 5 Merrion Square, Dublin 2, Ireland. [12]Service d'Astrophysique, DAPNIA/DSM/CEA, CE Saclay, F-91191 Gif-sur-Yvette, France. [13]Landessternwarte, Königstuhl, D-69117 Heidelberg, Germany. [14]Laboratoire d'Astrophysique de Grenoble, INSU/CNRS, Université Joseph Fourier, BP 53, F-38041 Grenoble Cedex 9, France. [15]Unit for Space Physics, North-West University, Potchefstroom 2520, South Africa. [16]Laboratoire de Physique Nucléaire et de Hautes Energies, IN2P3/CNRS, Universités Paris VI and VII, 4 Place Jussieu, F-75231 Paris Cedex 05, France. [17]Institut für Theoretische Physik, Lehrstuhl IV: Weltraum und Astrophysik, Ruhr-Universität Bochum, D-44780 Bochum, Germany. [18]Institute of Particle and Nuclear Physics, Charles University, V Holesovickach 2, 180 00 Prague 8, Czech Republic. [19]University of Namibia, Private Bag 13301, Windhoek, Namibia.

*Present address: Université Libre de Bruxelles, Faculté des Sciences, Campus de la Plaine, CP230, Boulevard du Triomphe, 1050 Bruxelles, Belgium.
†To whom correspondence should be addressed. E-mail: stefan.funk@mpi-hd.mpg.de
‡Present address: Department of Physics, Washington University, 1 Brookings Drive, CB 1105, St. Louis, MO 63130, USA.
§Present address: Department of Physics and Astronomy, University of Sheffield, Hicks Building, Hounsfield Road, Sheffield S3 7RH, UK.